Aircraft Observations of the Marine Boundary Layer Adjustment near Point Arguello, California

THOMAS R. PARISH

Department of Atmospheric Science, University of Wyoming, Laramie, Wyoming

DAVID A. RAHN

Atmospheric Science Program, Department of Geography, University of Kansas, Lawrence, Kansas

DAVE LEON

Department of Atmospheric Science, University of Wyoming, Laramie, Wyoming

(Manuscript received 14 May 2013, in final form 11 December 2013)

ABSTRACT

Northerly winds set up by synoptic conditions are persistent in the marine boundary layer (MBL) off the California coast from late spring through summer. Wind, pressure, and MBL height are modulated as the low-level flow impinges on the points and capes along the California coast. The Precision Atmospheric Marine Boundary Layer Experiment was conducted in May and June of 2012 with the primary goal to directly measure the dynamics responsible for the wind field near Point Arguello and Point Conception. Detailed measurements of the horizontal pressure field within the MBL were made using the University of Wyoming King Air research aircraft. Airborne measurements made during cases of strong northerly wind show an abrupt adjustment of the MBL near Point Arguello, including a modulation of the horizontal pressure gradient force and a near collapse of the MBL. Airborne lidar measurements complement measurements of the horizontal pressure field and help to elucidate the large changes in the MBL height in the vicinity of Point Arguello. The Weather Research and Forecasting Model was used to simulate the 20 May 2012 case at a high resolution. Model results showed large-amplitude height perturbations near Point Arguello, similar to those observed from the airborne platform. In this case, the offshore flow played an important role in the local forcing.

1. Introduction

Pronounced horizontal temperature gradients exist in the low levels of the atmosphere during the spring and summer months near the west coast of the United States. The Pacific high becomes established several hundred kilometers to the west of California over the relatively cool ocean, while a thermally driven low develops over the southwest. As a result, a strong horizontal pressure gradient persists through the warm season. Northerly winds are thus commonplace within the marine atmospheric boundary layer (MBL) adjacent to the West Coast from Washington to California. Beardsley et al. (1987), Zemba and Friehe (1987), Winant et al. (1988), Dorman and Winant (2000), Parish (2000), and others have described the wind regime based on standard observations (e.g., buoy data) and observations obtained during field campaigns. Others (e.g., Samelson and Lentz 1994; Burk and Thompson 1996; Koračin and Dorman 2001; Rahn and Parish 2007; Hsu et al. 2007) have used numerical simulations to examine the MBL wind and temperature fields near the California coast.

Coastal topography modulates the wind and pressure field adjacent to the coastline (e.g., Dorman 1985; Dorman et al. 1999; Edwards et al. 2001; Haack et al. 2001; Dorman and Koračin 2008). A strong subsidence inversion, forming as a consequence of the Pacific high, separates the relatively cool and moist marine air from the warmer and drier air in the free troposphere. During summer the MBL typically slopes upward to the west

Corresponding author address: Thomas R. Parish, Department of Atmospheric Science, University of Wyoming, 1000 E. University Ave., Laramie, WY 82071.
E-mail: parish@uwyo.edu

DOI: 10.1175/JAMC-D-13-0164.1

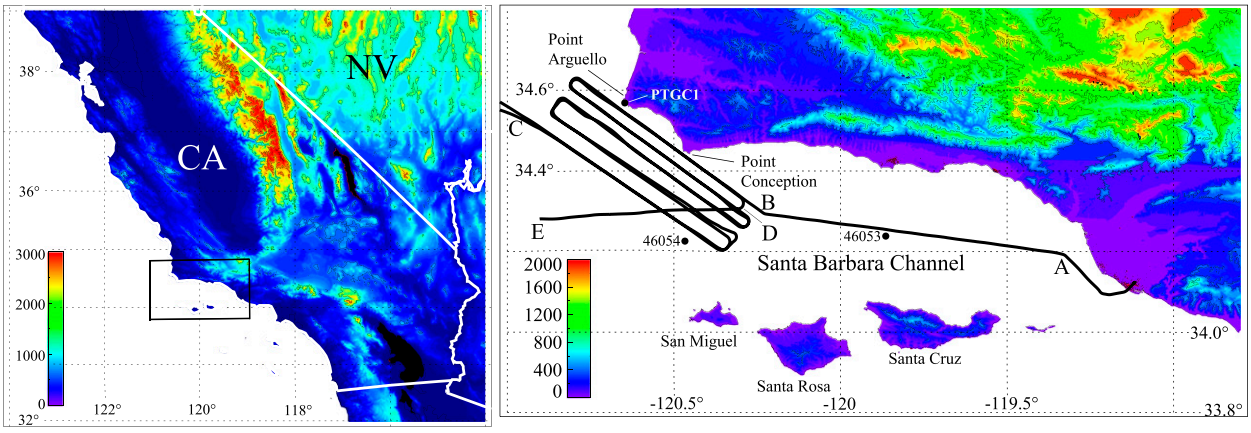

FIG. 1. (left) Topography and geographical features of PreAMBLE study area with (right) close-up view of boxed area near Point Arguello and Point Conception. Terrain contours are in meters. The King Air flight track for the 20 May 2012 case is indicated by the boldface labeled line.

from a depth of 100–200 m adjacent to the coast to 600 m or more ~100 km offshore (e.g., Parish 2000).

Several authors (e.g., Dorman 1985; Samelson 1992; Burk et al. 1999; Haack et al. 2001) represent the fluid system near the coast in terms of a two-layer shallow water model with the coastal terrain serving as a lateral boundary. The Froude number Fr characterizes adjustment of an unbalanced fluid flow, where Fr is defined as the ratio of the layer speed U to the fastest possible gravity wave in that layer:

$$\mathrm{Fr} = \frac{U}{\sqrt{g'H}}, \quad \text{where} \tag{1}$$

$$g' = g\frac{\theta_t - \theta}{\theta}. \tag{2}$$

The reduced gravity g' is defined using the acceleration of gravity g, the layer potential temperature θ, and the potential temperature of the inversion top θ_t. The speed of the fastest possible gravity wave is $\sqrt{g'H}$, where H is the depth of the layer. Discontinuities such as hydraulic jumps can result as the flow transitions from supercritical (Fr $>$ 1) to subcritical (Fr $<$ 1). As the flow in the MBL impinges on coastal points, significant modulation of the MBL height and wind field occurs. Blocking is observed on the upwind side and there is a local pressure increase. Downwind of the point, flow diverges and there is a pressure minimum that occurs in response to the divergence. From a hydraulic perspective, blocking manifests as a compression bulge; divergence is consistent with an expansion fan. Simulations of flow along the West Coast by Koračin and Dorman (2001) indicated compression bulges occur upwind of all major capes and points.

The most abrupt change in the California coastal terrain occurs at the Point Arguello and Point Conception headlands (see Fig. 1). Results from previous work (e.g., Dorman and Koračin 2008) suggest that the bend in the California coastline significantly modulates the MBL. The numerical simulations of Dorman and Koračin (2008) show a wind speed maximum is present that extends several hundred kilometers southwest of Point Arguello. A smaller wind speed maximum extends into the Santa Barbara Channel, which Dorman and Koračin (2008) attribute to an expansion fan in the lee of Point Conception.

Modeling of the marine environment near Point Arguello and Point Conception has been conducted by Skyllingstad et al. (2001) and Koračin et al. (2004). Skyllingstad et al. (2001) showed the importance of the large-scale horizontal pressure gradient force and MBL depth. They note that for a strong wind and a relatively deep MBL (~400 m), the flow exhibits supercritical characteristics.

Most observations of the flow come from fixed buoys near Point Arguello (see Dorman and Koračin 2008). Few airborne measurements have been conducted in the Point Arguello area with the notable exception of the missions conducted as part of Coastal Waves 1996 (Rogers et al. 1998). Observational results for the case on 20 May 2012 during the Precision Atmospheric Marine Boundary Layer Experiment (PreAMBLE), which was conducted from mid-May to mid-June 2012, are shown here. The primary goal of PreAMBLE was to study the atmospheric dynamics associated with the summertime MBL near the Point Arguello/Point Conception complex using the University of Wyoming King Air. The aircraft observations are compared to results from a finescale numerical simulation of this case conducted

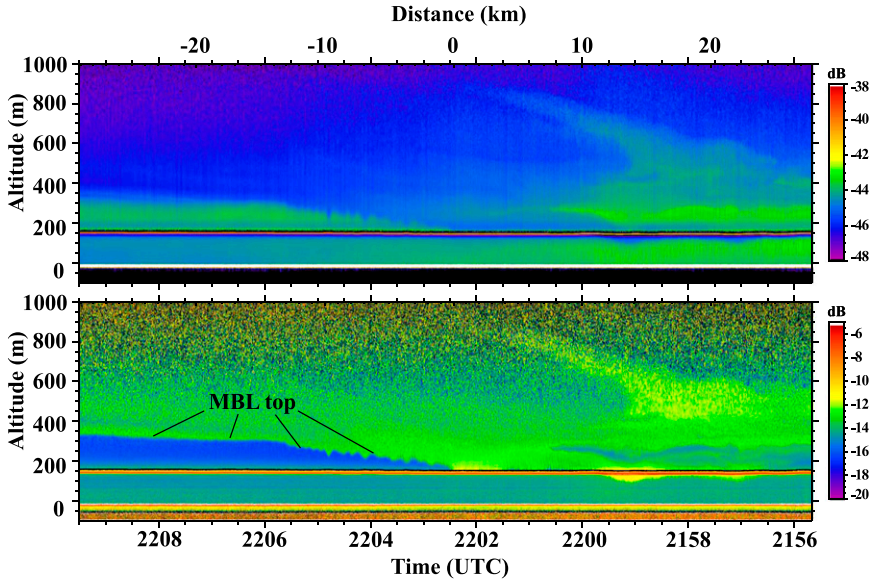

FIG. 2. Wyoming Cloud lidar image from 2156 to 2209 UTC 20 May 2012 showing (top) copolarized power (dB) and (bottom) depolarization ratio (dB). The King Air track is indicated by the solid horizontal line at 150 m.

using the Weather Research and Forecasting Model (WRF). For the 20 May 2012 case, WRF simulations used a 24-h simulation with a nested configuration consisting of four domains with the innermost grid centered over the Point Arguello–Point Conception headlands having a horizontal resolution of 1 km.

Two measurement capabilities are particularly important to this study: the horizontal pressure gradient force and measurements of backscatter and depolarization ratio from the Wyoming Cloud lidar. The King Air flight legs were typically conducted along isobaric surfaces. An independent measure of the height of an isobaric surface above some reference such as sea level is thus necessary. Since horizontal pressure fluctuations of about 0.1 hPa can be significant, the height of the aircraft static pressure port must be known to within a fraction of a meter. This accuracy has been achieved by differential GPS processing of King Air data (e.g., Parish et al. 2007; Parish and Leon 2013). Differential GPS requires deployment of one or more GPS reference stations. The reference GPS receiver, the position of which is known to a high degree of precision, is used to correct the GPS data collected on board the King Air. For PreAMBLE, a GPS base station receiver was deployed near the hangar housing the King Air at Point Mugu, California. Data were recorded at 10 Hz. Details of the differential GPS technique, sources of error, and limitations to the measurement accuracy are discussed in Parish and Leon (2013).

During PreAMBLE the King Air carried upward- and downward-looking versions of the Wyoming Cloud lidar. These lidars operate at 355 nm and are designed for retrieval of cloud and aerosol properties. The returned signal for the upward-looking lidar is sampled at 3.75-m intervals, while the signal for the downward-looking lidar is sampled at 1.5-m intervals Additional details of the upward- and downward-looking lidars can be found in Wang et al. (2009) and Wang et al. (2012). The lidar data are combined with the inertial navigation system/GPS data from the King Air to produce time–height images of the (uncalibrated) attenuated backscatter and the depolarization ratio (also uncalibrated). The lidars are well suited to determination of cloud boundaries, but the lidar signal is rapidly attenuated in cloud.

An example of the lidar copolarized power and depolarization ratio is shown in Fig. 2. Times in this and all subsequent figures are in UTC. The contrast in clear-air lidar returns from the aerosol, such as seen in Fig. 2, provides a means to infer the height of the MBL. The MBL is characterized by high backscattered power and low depolarization ratio as a result of higher concentrations of large aerosol, which have deliquesced as a result of their hygroscopicity and the ambient relative humidity. Immediately above the MBL top, the backscattered power decreases while the depolarization ratio increases. The depolarization ratio is of particular interest in that variations in the aerosol type can be detected, providing some insight into the air mass origin.

A high depolarization ratio suggests scattering from irregularly shaped particles such as dust or other dry aerosol. In contrast, deliquesced aerosols, which are inherently spherical, correspond to a low depolarization ratio. As a result of the strong contrast in depolarization ratio near the top of the MBL and the ability to detect subtle layering above the MBL, only depolarization ratio is shown in subsequent figures.

The King Air carried a Passive Cavity Aerosol Spectrometer Probe (PCASP) during PreAMBLE. Aerosol greater than about 0.1 μm in diameter can be detected by this instrument (Cai et al. 2013). While the PCASP provides size distributions from 0.1 to 3 μm, only the total aerosol concentration is used here.

Other key instrumentation onboard the King Air included a reverse flow thermometer and a Rosemount 102 sensor to measure air temperature (accuracy 0.5°C), an EdgeTech Vigilant model 137 to determine dewpoint temperature (accuracy 1°C), and a Rosemount 1501 High Accuracy Digital Sensing probe for static pressure (accuracy 0.5 hPa). Winds are determined from a Rosemount 858 five-hole gust probe mounted on the King Air (e.g., Lenschow et al. 1991) and have been corrected using the onboard GPS (accuracy $< 1\,\mathrm{m\,s^{-1}}$). Two GPS receivers, an Ashtech Z-Sensor and a Trimble netRS, are installed on the King Air and are used in the differential correction process to determine the three-dimensional position of the aircraft. Differential corrections were computed using the commercial package GrafNav 8.10 from NovAtel, Inc.

2. PreAMBLE case for 20 May 2012

The primary goal of PreAMBLE was to examine the atmospheric dynamics associated with the summertime MBL near the Point Arguello–Point Conception complex. Results from previous work (e.g., Dorman and Koračin 2008) suggest that the topographic bend in the California coastline significantly modulates the MBL. Figure 3 illustrates the May–June 2008–09 mean 1000-hPa height, wind speed, and streamlines based on the operational National Centers for Environmental Prediction (NCEP) ~5-km High-Resolution Window Forecast System (HIRESW). The large-scale atmospheric circulation (Fig. 3a) is dominated by the Pacific high with flows from the north across the entire eastern Pacific. Horizontal pressure gradients are enhanced near the California coast with maximum 1000-hPa winds extending from Cape Mendocino to San Francisco. Although the maximum 1000-hPa wind is found in the marine environment over northern California, the $8\,\mathrm{m\,s^{-1}}$ isotach (Fig. 3a) extends along the entire California coastline past Point Arguello.

In their month-long simulation (using a 9-km horizontal grid scale) Dorman and Koračin (2008) noted a similar feature with the strongest winds at the surface immediately adjacent to the coast. They interpreted this maximum to be the result of an expansion fan as flows impinged on Cape Mendocino. This section of the California coastline is closest to the center of the Pacific high. The strong temperature contrast between the land and ocean further enhances the horizontal pressure gradient force (e.g., Beardsley et al. 1987; Parish 2000).

As the mean 1000-hPa northerly wind regime impinges on the coastline in the region of Point Arguello, the flow turns slightly eastward (Fig. 3b). Parish et al. (2013) note that cyclonic vorticity within the California Bight region was commonplace during PreAMBLE. An eddy circulation detectable in the satellite imagery occurred on 24 out of the 33 days during the field experiment. The 1000-hPa surface heights also display a turning around Point Arguello and a tight gradient in the western Santa Barbara Channel. A weak local maximum in the 1000-hPa wind speed occurs just south of Point Arguello similar to the June 1999 climatology reported by Dorman and Koračin (2008). Rapid deceleration of the wind occurs from west to east along the axis of the Santa Barbara Channel, despite the relatively strong pressure gradient force.

On 20 May 2012, The King Air conducted a series of flight legs in the lower atmosphere near Point Arguello. To measure the horizontal pressure field, the King Air flew a repeating, ladder pattern centered over the western edge of the Santa Barbara Channel. This flight track is shown in Fig. 1. After takeoff from Point Mugu, the King Air proceeded west within the Santa Barbara Channel, conducting a series of five vertical soundings between 200 and 800 m from points A to B depicted in Fig. 1. To ensure accurate wind measurements, ascent and decent rates were limited to about $3\,\mathrm{m\,s^{-1}}$. Thus, at the normal King Air flight speed of $90\,\mathrm{m\,s^{-1}}$, each sounding required about 3 min and corresponds to a horizontal displacement of about 16 km.

At the end of the Santa Barbara Channel (point B) the King Air flew at a 300° heading to begin the ladder pattern. This pattern consisted of five isobaric legs, each at a height of approximately 150 m above the ocean. Each segment of the ladder pattern was about 60 km in length with an offset of 4–5 km between successive segments. After the five-leg pattern was completed near point C, soundings were conducted in the MBL along the same track. Following completion of the sounding leg, the ladder pattern was repeated in reverse. This was followed by additional soundings between points D and E shown in Fig. 1. Because of fuel constraints, the King Air returned directly to base after reaching point E.

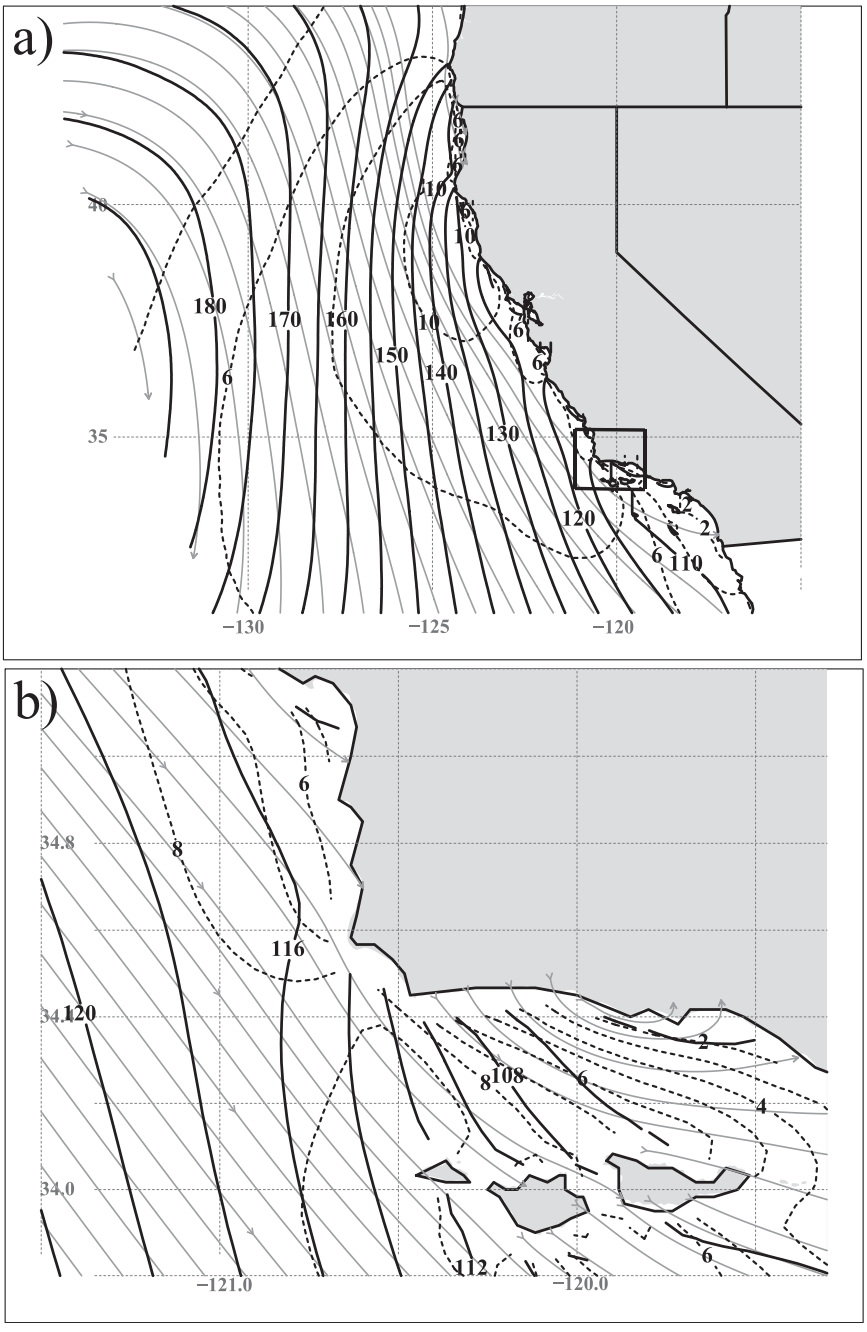

FIG. 3. (a) Mean May–June 2008–09 1000-hPa field of height contours (thick line; m), wind speeds (dashed lines; m s^{-1}), and streamlines (solid gray lines) based on NCEP HIRESW for marine environment off the California coast with (b) close-up of boxed region near Point Arguello–Point Conception in Southern California.

3. King Air observations

a. Overview

Figure 4 illustrates the large-scale conditions on 2100 UTC 20 May 2012 from the 0.5° × 0.5° grid Climate Forecast System Reanalysis (Saha et al. 2010). In comparison with the mean conditions illustrated in Fig. 3, conditions were anomalous in several ways. A relatively deep upper-level low was situated over the North Pacific at 500 hPa (Fig. 4a) with ridging over the western United States. The Pacific high in the lower levels (Figs. 4b–d) shifted southward from its climatological

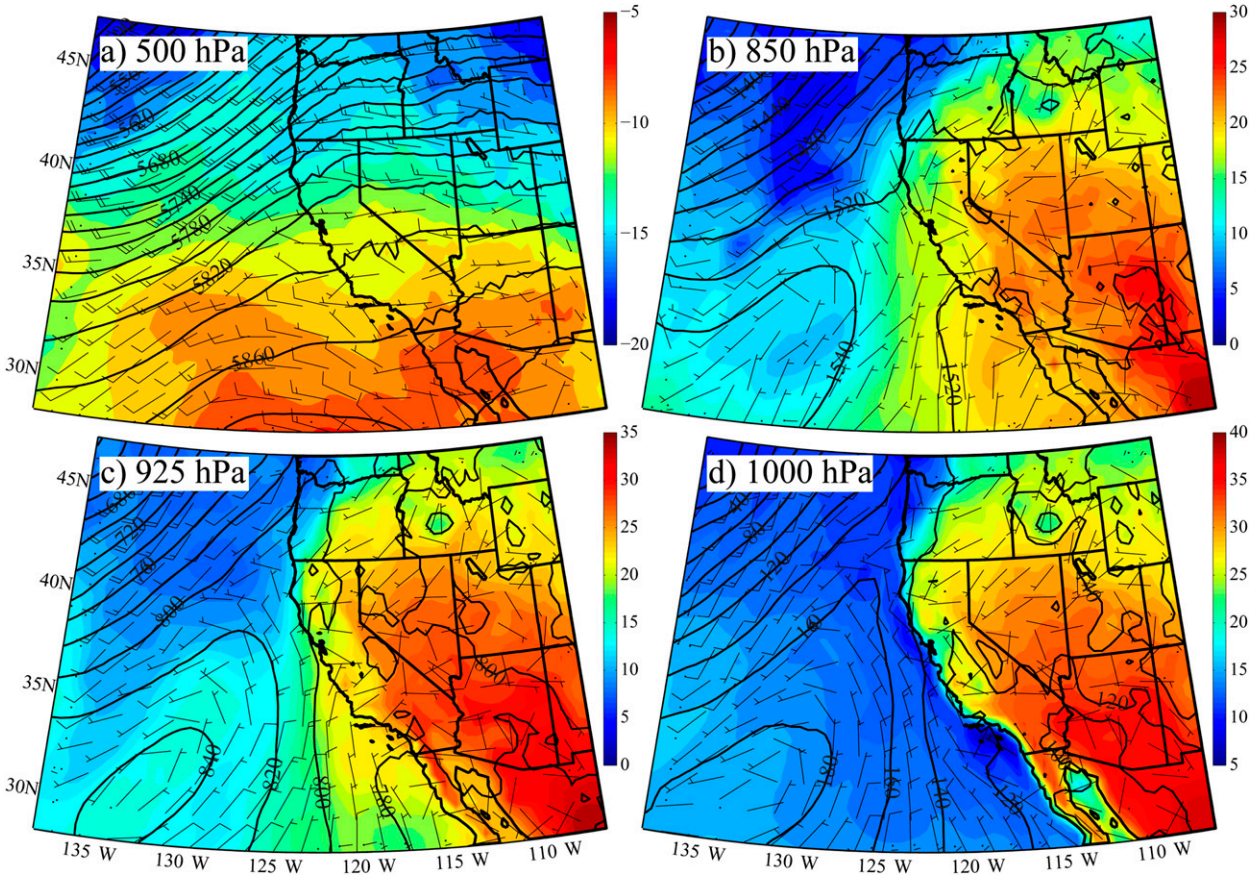

FIG. 4. Geopotential height (m; contours), temperature (C; shading), and wind barbs ($m\,s^{-1}$) at 2100 UTC 20 May 2012 for (a) 500, (b) 850, (c) 925, and (d) 1000 hPa from the Climate Forecast System Reanalysis.

position in response to the large cyclonic circulation in the North Pacific such that the center of the anticyclonic circulation is about 1000 km west of Baja California. The cold-core nature of the high pressure is apparent and thus the anticyclonic circulation decreases with height.

Southwest winds are present at 500 hPa over most of the West Coast. The zone of northerly winds at 1000 hPa reaches a maximum offshore from Southern California with weak flow from Cape Mendocino northward. Even at the scale shown in Fig. 4, turning of the 1000-hPa wind within the California Bight is apparent. A Catalina eddy circulation was present in the morning hours of 20 May 2012 as revealed by a cyclonic circulation of the low stratus in the eastern half of the bight. Surface station PTCG1 is situated at the coast near Point Arguello (see Fig. 1) and indicated a northerly wind throughout the duration of the flight on 21 May. The mean hourly wind speed from PTCG1 increased from 6 $m\,s^{-1}$ near the start of the flight at 2100 UTC to 10 $m\,s^{-1}$ near the end of the flight at 0000 UTC. Buoy 46054 is located at the western end of the Santa Barbara Channel (see Fig. 1) and indicated that the mean hourly winds from about 300° increased over the duration of the flight from 6.4 $m\,s^{-1}$ at 2100 UTC to 12.5 $m\,s^{-1}$ 3 h later.

b. *Structure of the lower atmosphere in the Santa Barbara Channel*

The King Air departed Point Mugu at 2030 UTC, heading west within the Santa Barbara Channel. Satellite imagery revealed a Catalina eddy circulation in the early morning with extensive cloud coverage in the eastern California Bight. The center of circulation was about 50 km south of Santa Cruz Island, and a comma-shaped cloud structure extended across the Santa Barbara Channel past Santa Rosa Island. With daytime heating, the clouds began to dissipate. By the end of the aircraft mission in the early afternoon, clouds had thinned considerably. West of the Channel Islands, clear skies persisted throughout the flight.

After takeoff, the King Air climbed to about 1000 m and took a series of vertical profiles to document the MBL structure. The depolarization ratio from the lidar and corresponding vertical profiles of temperature and wind in the layer from near cloud top to ~(800–1000) m are

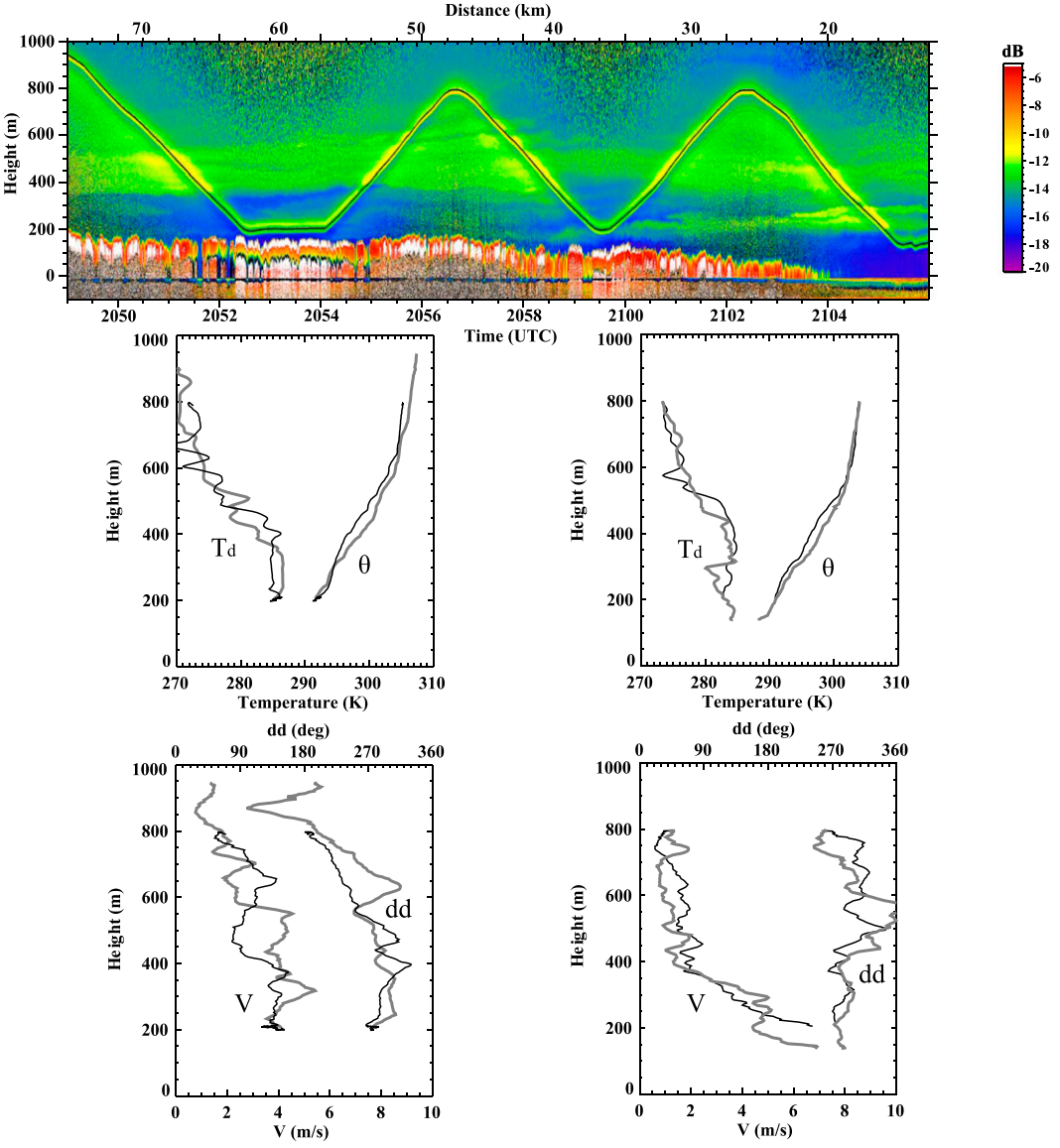

FIG. 5. King Air data collected during westward sounding traverse along Santa Barbara Channel for 2050–2104 UTC 20 May 2012. (top) Depolarization ratio (dB) from Wyoming Cloud lidar with flight track superimposed. (middle), (bottom) Data from the (left) first two soundings and (right) last two soundings with ascent profiles in thick gray lines and descent profiles in thin black lines: dew point (T_d; K) and potential temperature (θ; K), and wind speed (V; m s^{-1}) and direction (dd; °), respectively.

shown in Fig. 5. A thin cloud layer associated with the weakening Catalina eddy circulation was present with cloud tops about 150 m above the ocean. Cloud top is evident in the lidar data. Soundings revealed a gradual increase in potential temperature above cloud top.

Since the King Air did not penetrate into the lowest layer, surface data are used to infer the temperature inversion strength. Surface air temperatures at the closest time from buoys 46053 and 46054 are 286 and 287 K, respectively. The lowest recorded temperature just above the cloud top at about 200 m is ~290 K, so the inversion strength is only 3–4 K.

Lidar depolarization ratios indicated subtle layering at around 350–400 m above the surface. Cloud-top height gradually decreased westward prior to the cloud field dissipating completely during the westernmost sounding profile. Wind speeds were less than 5 m s^{-1} until the lowest levels of the final two soundings. The increase in wind speed likely indicates the top of the marine layer. Wind directions within the lowest 500 m

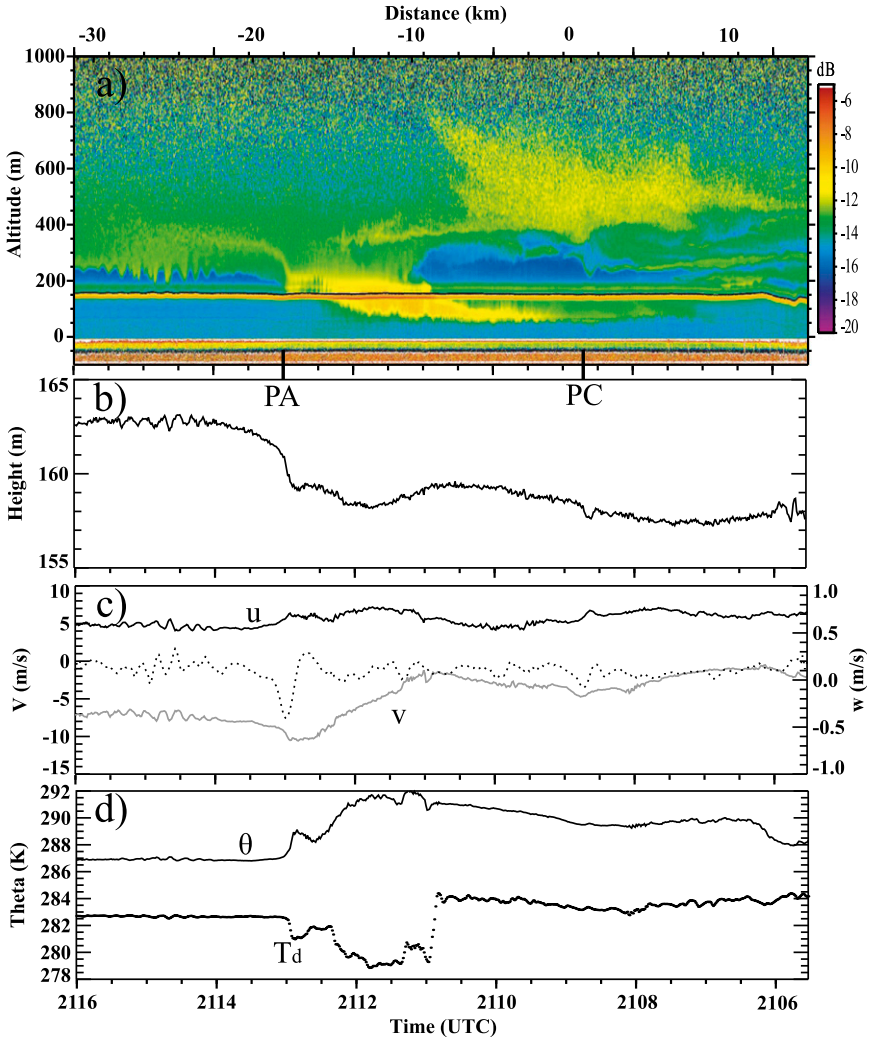

FIG. 6. King Air measurements from leg 1 (closest to headlands in map shown in Fig. 1) at the 995-hPa level from 2106 to 2116 UTC 20 May 2012 of (a) depolarized lidar return from lidar (dB); (b) 995-hPa isobaric heights (m); (c) wind components (m s^{-1}) u (black line), v (gray line), and w (dashed line, axis to right); and (d) potential temperature (K) and dewpoint temperature (K). Position along flight track closest to Point Arguello (PA) and Point Conception (PC) indicated by the solid tick marks on the x axis in (a); northwest is to left.

above the Santa Barbara Channel were from about 300°. After the fifth sounding, the King Air was positioned near point B in Fig. 1 and the isobaric mapping commenced.

c. *Mapping the marine boundary layer structure near Point Arguello*

The King Air mapping pattern was aligned along the mean wind with a heading of 307° for the first leg and flown about 160 m above the ocean. No clouds were present during the mapping mission. King Air measurements for the first leg, 2105–2116 UTC, passing closest to the headlands of Point Arguello and Point Conception, are summarized in Fig. 6. Changes in the MBL depth which are apparent from the lidar depolarization ratio (Fig. 6a) are documented. West of Point Conception, the King Air flight level is clearly within the MBL, while from Point Arguello to the eastern end of the leg the King Air flight track is above the top of the MBL. MBL thickness decreases sharply east of Point Arguello, dropping from about 250 m to less than 100 m over a distance of about 5 km.

Lidar depolarization ratios also suggest profound differences in aerosol characteristics along the leg between Point Conception and Point Arguello, consistent with a transition from maritime (lower depolarization

ratios, west of Point Arguello) to continental (higher depolarization ratios, east of Point Arguello) sources of aerosol. Instrumentation onboard the King Air supports the assertion that the high depolarization ratio values were associated with continental aerosol. PCASP total aerosol concentration measurements showed step changes corresponding to depolarization ratio boundaries such as those indicated in Fig. 6a near Point Arguello. MBL aerosol total concentrations as measured by the PCASP were typically 150–190 cm^{-3}. As the King Air crossed the MBL boundary east of Point Arguello, PCASP total concentration increased to nearly 400 cm^{-3}. The jump in aerosol concentration is consistent with a transition from a marine to continental air mass.

King Air measurement of the 995-hPa heights as inferred from differential GPS processing is shown in Fig. 6b. Trends in the isobaric heights are consistent with features in the lidar depolarization ratio. A 4-m isobaric height decrease (corresponding to a horizontal pressure decrease of about 0.5 hPa) occurs over a distance of less than 5 km just east of Point Arguello. Note that the waves evident in the lidar image at the MBL top west of Point Arguello are reflected in the isobaric height field. Close inspection reveals that the waves detected by the lidar are in phase with the isobaric height perturbations. These waves have amplitudes of about 1 m, equivalent to a horizontal pressure perturbation of about 0.12 hPa.

Wind speeds decrease from west to east (Fig. 6c) reaching a maximum just east of Point Arguello where the temperature inversion that caps the MBL is crossed. This is consistent with accelerations in response to the increased slope of the isobaric surface. The magnitude of the y component of the wind decreases from 10 to 2–3 m s^{-1} just east of Point Arguello. Pronounced changes in vertical motion are observed near the point of the greatest MBL slope. Gravity waves west of Point Arguello are evident in the lidar image (Fig. 6a); all three wind components reflect perturbations apparently tied to the gravity waves.

Potential temperatures measured by the King Air (Fig. 6d) are consistent with the position of the King Air within or above the MBL. The King Air is within the MBL west of Point Arguello, and conditions are cool and moist. To the east of Point Arguello, the King Air is above the MBL and warm temperatures and low dewpoints are observed. Note that the high depolarization ratio just west of the MBL slope is linked to higher potential temperatures and relatively low dewpoints. Such conditions are consistent with aerosol of continental origin.

Froude number calculations have been made using data collected from the King Air within the MBL west of Point Arguello. Here a mean layer wind speed of 10 m s^{-1} is used. The potential temperature difference between the MBL and free atmosphere is about 5 K and the MBL height is about 250 m. These values yield a Froude number of 1.7, suggesting that supercritical conditions are present in the MBL. Supercritical conditions imply that gravity wave disturbances are unable to propagate upstream. Unlike measurements from other days that show a clear compression bulge before the drop of the MBL (Rahn et al. 2013), no evidence of blocking is present on this day. The MBL thickness and height of the isobaric surface upstream of Point Arguello are essentially flat.

After the initial southeast-to-northwest leg, the King Air turned and conducted a second leg (2118–2129 UTC) along the same axis and at the same 995-hPa level, but from northwest to southeast and offset from the previous leg by about 4 km (Fig. 1). Airborne measurements for this leg are summarized in Fig. 7. Lidar imagery (Fig. 7a) again shows the along-leg trend in the MBL height with the most significant change seen adjacent to Point Arguello. Wave activity is again present at the MBL top. Lidar images suggest layering between Point Arguello and Point Conception such that continental aerosols are situated just below the MBL top with aerosol of possibly marine origin just above the MBL.

There again appears to be a collapse of the MBL and a clearly defined minimum in MBL thickness with a top only about 100 m above the ocean east of Point Arguello. Isobaric heights (Fig. 7b) display a similar trend as the previous leg with a shallower slope near Point Arguello. Layering seen in the lidar depolarization ratios is mirrored in the isobaric heights between Point Arguello and Point Conception with a local height maximum of 1–2 m that is tied to the elevated marine layer.

Wind (Fig. 7c), potential temperature, and dewpoint (Fig. 7d) follow similar trends to the previous leg. Maximum wind speeds again are observed near Point Arguello, near the steep isobaric slope. A region of high depolarization ratio is seen east of Point Arguello and is coincident with low dewpoint temperatures. PCASP total aerosol concentration measurements are similar to those from the initial leg.

Legs 3–5 of the mapping mission (not shown) revealed similar trends to those shown in Figs. 6 and 7. There is a gradual smoothing of the gradients in MBL height and isobaric height for the legs farther away from the coastline. The strongest winds are seen near the point of the MBL collapse. The MBL depth increases for the legs farther offshore. The King Air flight track at 995 hPa was contained almost entirely within the MBL for the leg farthest to the southwest. The lidar example images shown in Fig. 2 are from the final leg of the mapping pattern.

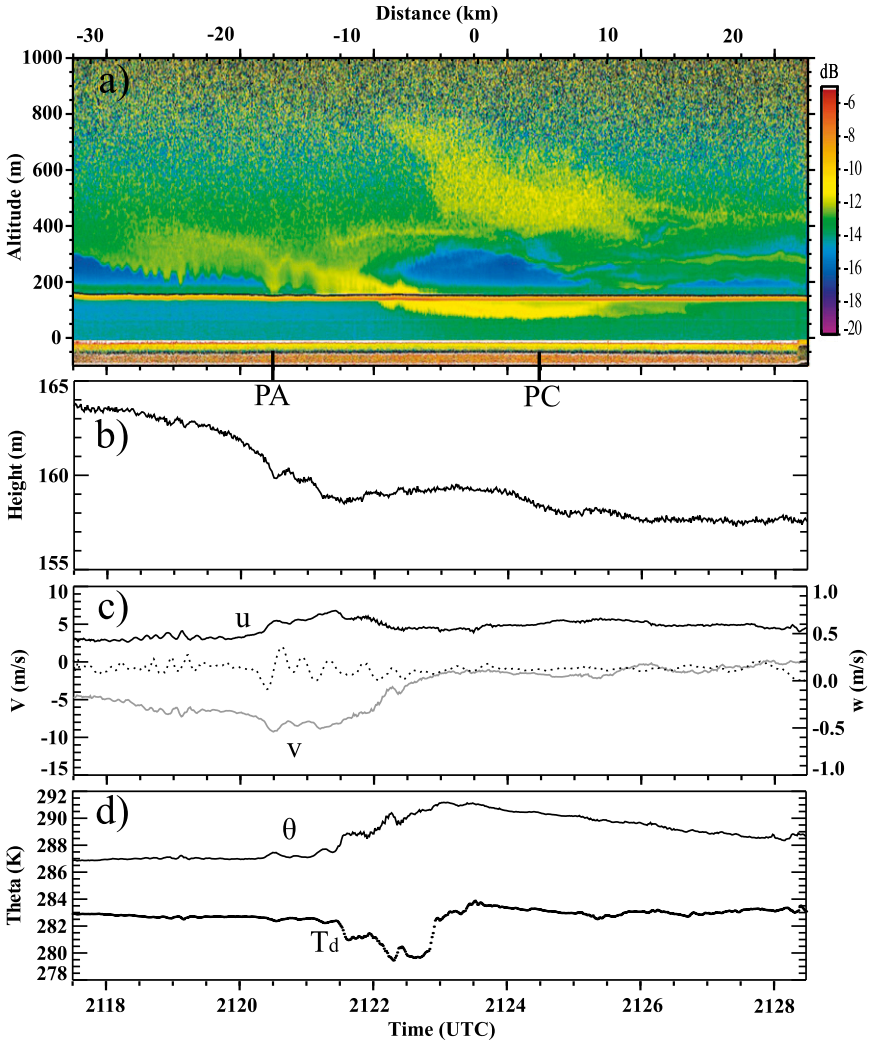

FIG. 7. As in Fig. 6, but for leg 2 (second closest to headlands) from 2118 to 2128 UTC.

King Air data for the entire pattern are summarized in Fig. 8, which shows the spatial fields of MBL height inferred from the lidar, isobaric height, wind speed, and potential temperature. MBL heights (Fig. 8a) display a westward increase with the most pronounced change near Point Arguello. Isobaric heights (Fig. 8b) show the largest gradient near Point Arguello. The strongest winds (Fig. 8c) are found along the zone where the horizontal pressure gradient is largest. Although heights continue to decrease eastward, the wind speeds decrease. At the western edge of the Santa Barbara Channel, winds are nearly parallel to the isobars and are in a quasi-geostrophic balance.

King Air measurements of potential temperature (Fig. 8d) are strongly influenced by aircraft position with respect to the MBL top. Large potential temperature gradients are observed as the plane crosses temperature inversion that marks the top of the MBL. Little variation in potential temperature was observed once the King Air was within the well-mixed MBL.

After completion of the first mapping pattern, soundings were obtained near point C in Fig. 1, which is situated west of the Santa Barbara Channel. Four ascents and descents were conducted: the first two from the 2209–2215 UTC period with the King Air heading west and the last two from the 2215–2230 period with the King Air heading back east. MBL heights increase only slightly toward the west and all soundings reveal the classic MBL structure. Figure 9 shows the lidar depolarization ratios and corresponding profiles of temperature, dewpoint, and wind speed and direction. A well-defined low-level jet was observed near the top of the MBL.

d. Second MBL mapping pattern

Observations from buoys at Point Arguello and at the western end of the Santa Barbara Channel indicated an

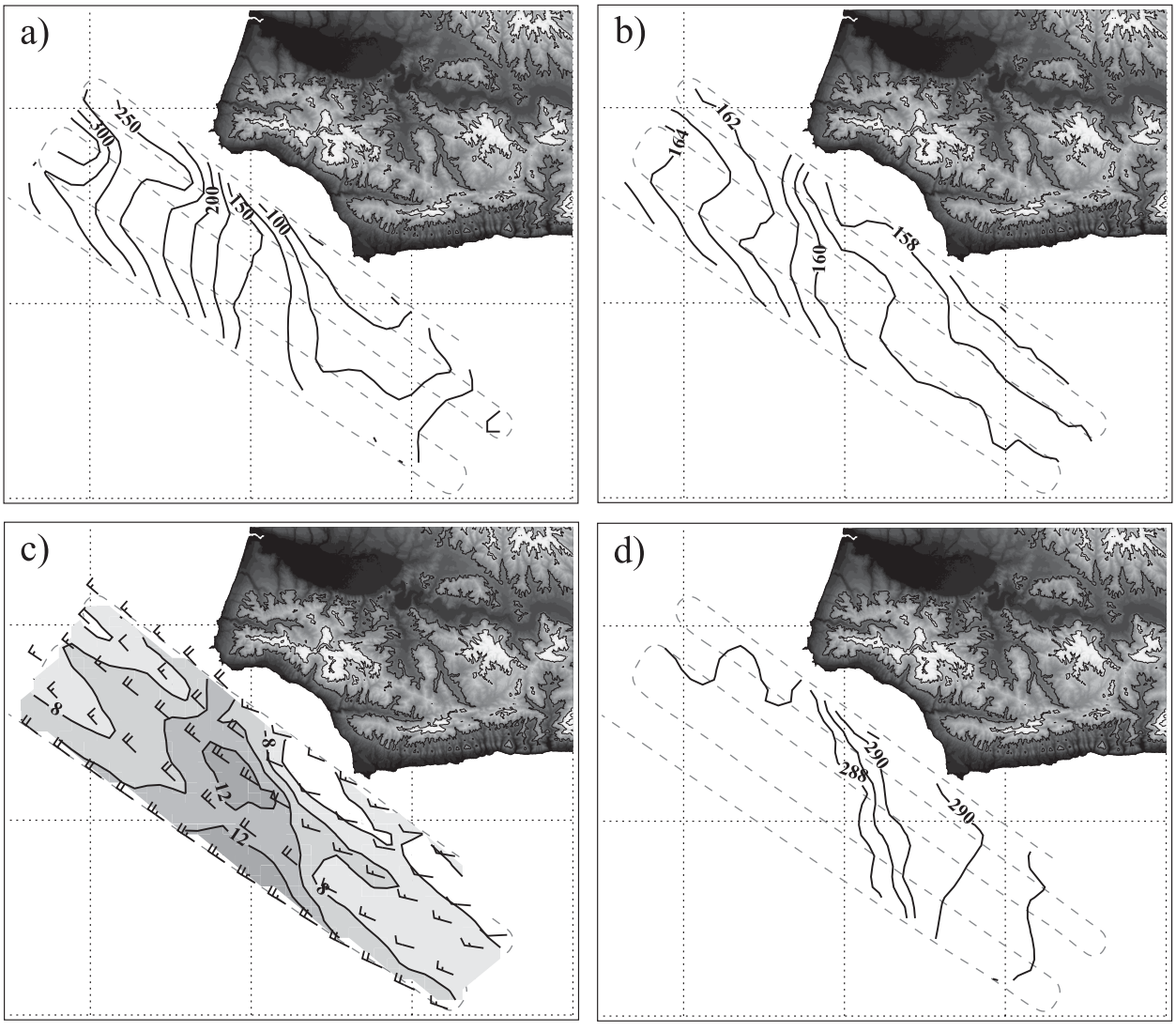

FIG. 8. Summary of King Air measurements off of Points Arguello–Conception headlands for first mapping pattern (diagonal dashed lines in each panel are the flight track) on 20 May 2012 from 2105 to 2210 UTC: (a) MBL heights (m) at 25-m increments estimated from lidar; (b) 995-hPa level isobaric height field (m) at 1-m increments based on differential GPS data; (c) wind speeds (color shaded contours; $m\,s^{-1}$) at increments of $1\,m\,s^{-1}$ with wind barbs (large barb is $5\,m\,s^{-1}$); and (d) potential temperatures (K) at increments of 1 K.

increase in the surface wind from the 2200–2330 UTC period coincident with the second ladder pattern. Increasing wind speeds were also seen in the King Air observations. Such changes in wind generally indicate an increase in the magnitude of the regional horizontal pressure gradient; thus the adjustment near Point Arguello should be accentuated compared to observations from the first mapping pattern. The sequence of legs conducted during the second ladder pattern was opposite to that of the first. Thus the King Air sampled the section of coastline nearest Point Arguello and Point Conception during the final leg. As with the first ladder pattern, the amplitude of the isobaric changes increased as the aircraft approached the headlands. The largest changes in MBL height, wind, and temperature occurred when the aircraft was closest to Point Arguello.

Figure 10 summarizes the King Air observations for the final leg of the second mapping pattern. MBL heights as inferred from the lidar depolarization ratios (Fig. 10a) show a pronounced change from a height of about 350 m just west of Point Arguello to a near collapse of the MBL with heights less than 50 m between Point Arguello and Point Conception. Wave activity is again seen at the MBL top. A pronounced MBL height gradient is present in the lidar imagery approximately 5 km east of Point Arguello, where heights abruptly change by 200 m.

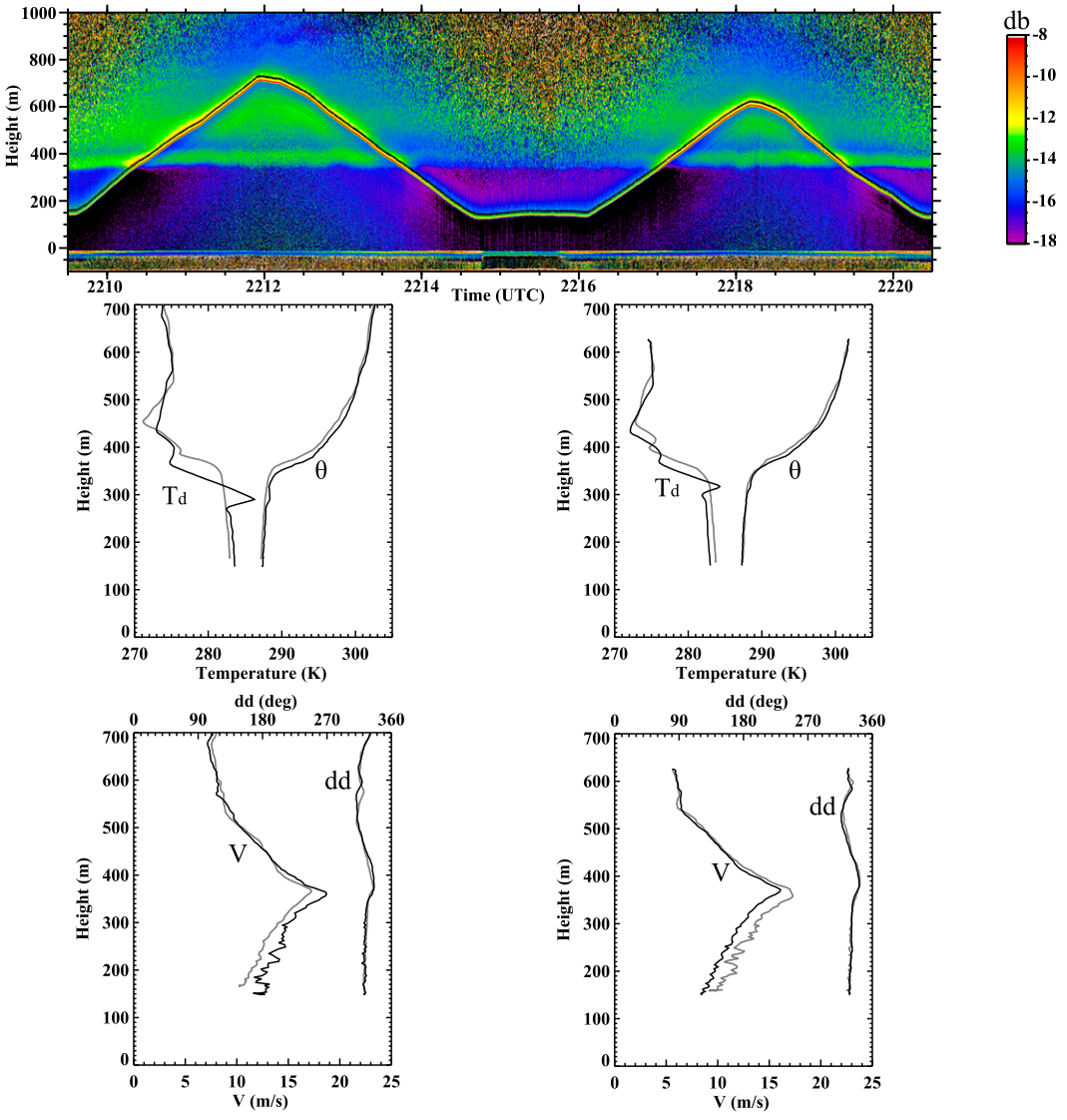

FIG. 9. As in Fig. 5, but for data collected west of Point Arguello near point C shown in Fig. 1 from 2209 to 2221 UTC 20 May 2012.

Isobaric surface heights (Fig. 10b) show a marked decrease east of Point Arguello of nearly 10 m over less than a 5-km horizontal distance, corresponding to a horizontal pressure change of about 1.2 hPa. This change, occurring over 5 km, is equivalent to a geostrophic wind of about 250 m s^{-1}, and thus large accelerations should be present. Isobaric height changes are about twice as large as what were seen during the first leg of the initial ladder pattern. A local height maximum of about 2.5 m is detected as the King Air travels through the height discontinuity just east of Point Arguello, consistent with the physical picture inferred from the lidar image. As the King Air moves eastward past Point Conception, isobaric heights increase such that by the eastern end of the leg the MBL top is near flight level.

Of special interest are the high depolarization ratios seen from east of Point Arguello to beyond Point Conception, suggesting an enhancement of the dry aerosol as compared to the initial leg. PCASP total concentration numbers again indicate a step change from about 150 cm^{-3} in the marine layer to 380 cm^{-3} just east of Point Arguello, consistent with the observed increase in lidar depolarization ratio. This strongly suggests continental influence in the layer above the MBL between Point Arguello and Point Conception, and implies that significant offshore flow on the scale of tens of kilometers is present. Implications of the offshore flow in terms of

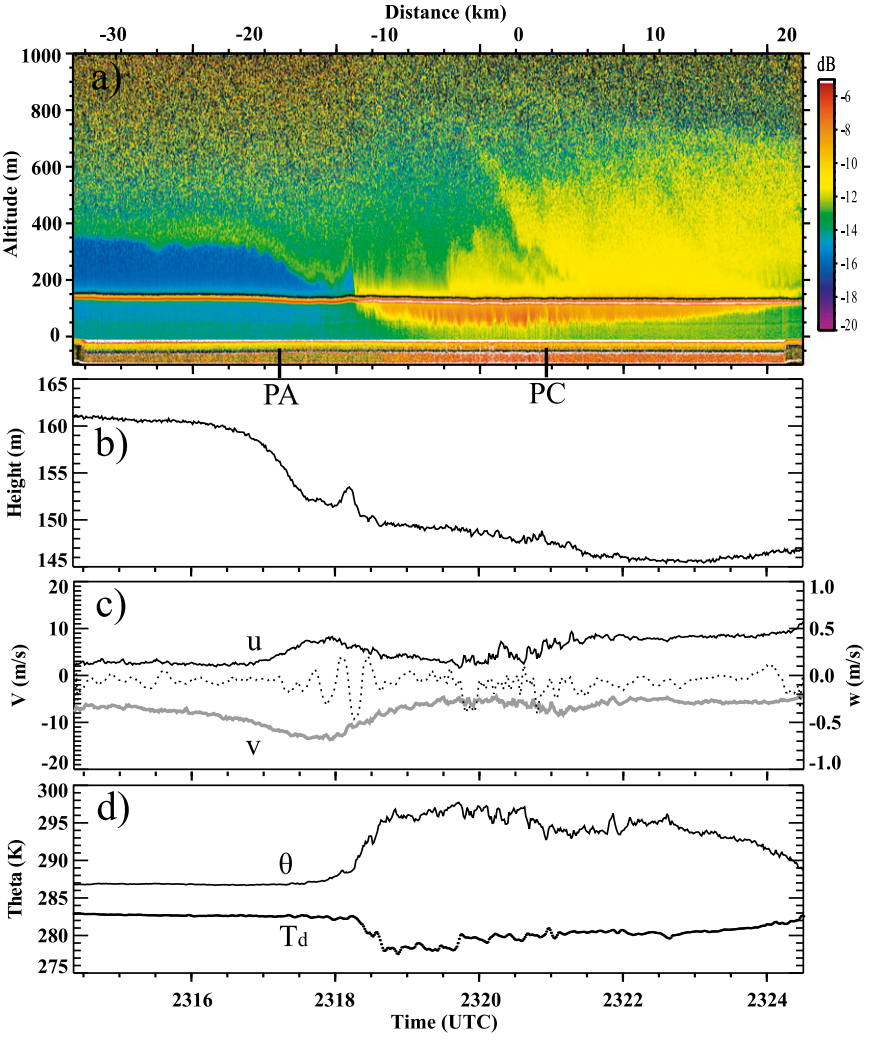

FIG. 10. As in Fig. 6, but for the leg from 2314 to 2325 UTC.

the dynamics of the sudden changes in the MBL height will be discussed later.

Winds within the MBL (Fig. 10c) are considerably stronger than those observed during the first mapping sequence. Wind speeds reach 16 m s^{-1} east of Point Arguello. Interpretation of the wind is straightforward when viewed in the context of the position of the King Air with respect to the MBL top. West of Point Arguello the King Air passes through the MBL. Maximum wind speed corresponds to the steepest isobaric slopes. East of the MBL rise, wind speeds (Fig. 10c) decrease as the King Air passes into the free atmosphere. There seems no doubt that wind speeds within the MBL below flight level downstream of the MBL slope must be greater than those observed upstream. Downward-looking video recorded during the flight showed a highly agitated ocean surface. Vertical velocities show a significant downward motion in response to the MBL collapse and strong perturbations associated with the pronounced jump in the MBL inferred from the lidar depolarization ratio cross sections and isobaric heights.

Potential and dewpoint temperatures (Fig. 10d) displayed trends consistent with the path of the King Air from within the MBL along the western end of the leg to the free atmosphere downstream of Point Arguello. The gradient in potential temperature from the MBL to the free atmosphere has increased by about a factor of 2 from that seen earlier. The vertical temperature gradient shown in Fig. 10d is greater than that from the initial leg from the first mapping mission (Fig. 6d). The increase must be due to warm air above the MBL since the temperature remains at about 287 K within the MBL.

Throughout both ladder patterns, the largest MBL adjustment is tied to the coastal headlands at Point Arguello. A summary of the King Air observations from the second mapping pattern is shown in Fig. 11. As with

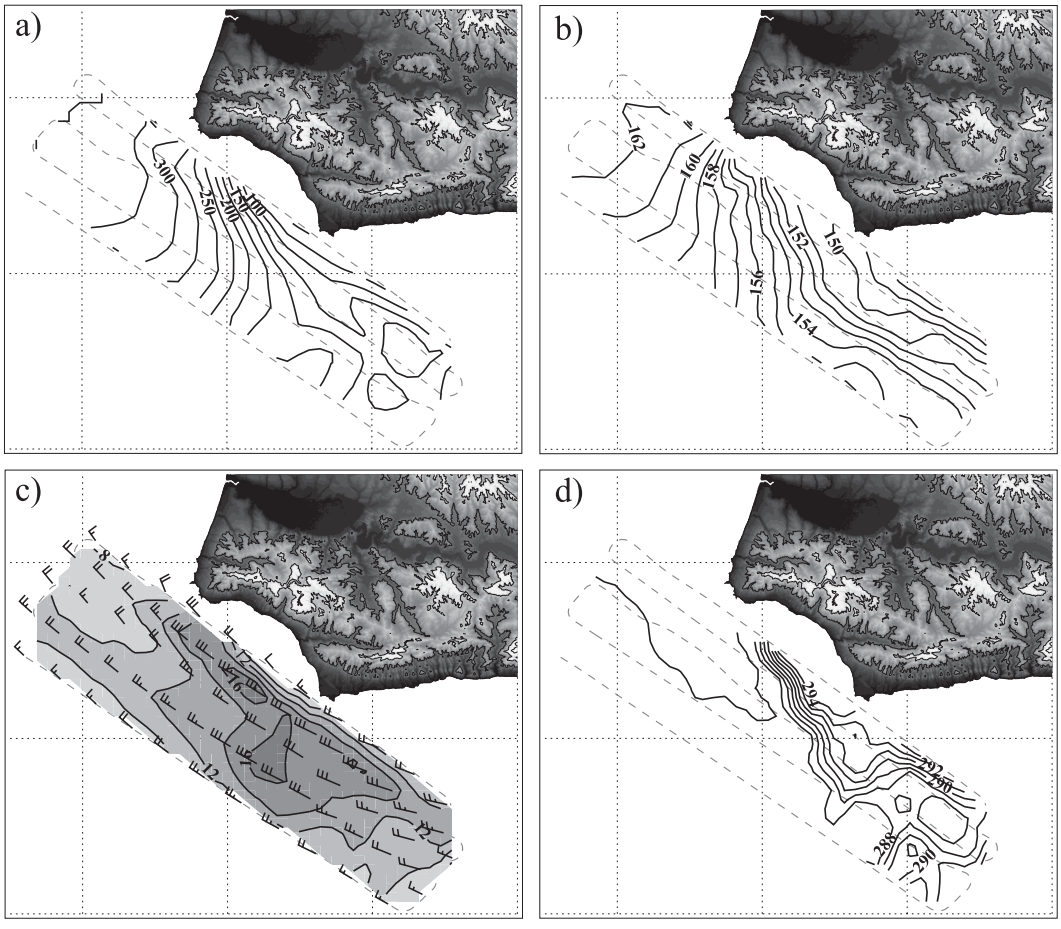

FIG. 11. As in Fig. 8, but for the second mapping pattern from 2220 to 2325 UTC.

the first mapping pattern (Fig. 8), marine-layer heights increase to the west. The magnitude of the MBL height change is larger than that seen in the first mapping pattern. MBL heights (Fig. 11a) increase from 100 to 300 m over about 10 km for the three legs closest to the headlands. An increase in the horizontal pressure gradient is apparent as indicated by the isobaric height field (Fig. 11b), corrected for observed isallobaric tendencies (e.g., Parish et al. 2007). Although the height gradient has increased, the overall pattern remains similar to what was seen during the previous set of legs 2 h earlier. The focus of the height change was centered on Point Arguello.

The strongest wind speeds (Fig. 11c) are situated along the zone of the strongest horizontal pressure gradient force. Significant cross-isobar flow is apparent near the speed maximum, implying a nongeostrophic response just west of the Santa Barbara Channel. At the eastern end of the mapping pattern, wind vectors are roughly parallel to the height contours but wind speeds are considerably subgeostrophic. Wind vectors in Fig. 11c do not show evidence of significant diffluence, as would be expected in the case of an expansion fan, but rather suggest weak confluence near Point Arguello. This suggests that the sudden collapse of the MBL may not be solely the result of expansion fan dynamics. Potential temperatures can again be interpreted with respect to the MBL height with little variation to the west where King Air is within the MBL, but with a tight gradient to the east as the plane crosses the temperature inversion that caps the MBL.

4. WRF simulations of the 20 May case

Real-time simulations of the MBL near the Point Arguello–Point Conception headlands were conducted using WRF throughout the PreAMBLE field experiment. Results of such modeling work are considered invaluable because they reveal the larger-scale processes at work in which the King Air observations are embedded. Extensive work has been conducted that compared the King Air observations with the WRF

output, and those results have guided the choice of parameterization schemes. As with previous modeling studies of the MBL such as described by Rahn and Parish (2008), the choices of planetary boundary layer and cloud parameterizations critically influence the entire wind and temperature fields including propagation of cloud features along the coast.

The simulation of the 20 May 2012 case shown here has been completed using version 3.3.1 of WRF, but simulations have also been conducted with version 3.4.1 [for a complete description of the WRF model, see Skamarock et al. (2008)]. Practically no difference between the versions was detected for the same suite of parameterization schemes. After the field campaign ended, a model domain consisting of four nested domains with resolutions of 27, 9, 3, and 1 km centered over the Point Arguello–Point Conception complex was used. The innermost domain consists of 151 × 151 grid points. A vertical grid of 70 sigma levels is used with increasing resolution toward the surface. Key parameterizations used for the run are the following: Lin (Purdue) microphysics scheme, Goddard scheme for longwave radiation physics, Dudia shortwave radiation scheme, Fifth-generation Pennsylvania State University–National Center for Atmospheric Research Mesoscale Model (MM5) surface layer similarity with the unified Noah land surface model, and the Yonsei University boundary layer physics scheme.

Extensive sensitivity testing was conducted concerning the low stratus clouds observed during episodes of the Catalina eddy circulation that occurred frequently during PreAMBLE. This follows from the comprehensive evaluation of WRF in simulating King Air measurements associated with a coastally trapped wind reversal (e.g., Rahn and Parish 2008, 2010). For the case of the coastally trapped wind reversal, WRF was able to capture the thermodynamic and dynamic structure of the atmosphere and correctly simulate the distribution and evolution of the observed stratus. For this case, the model was initialized at 0000 UTC 20 May 2012 using the operational National Centers for Environmental Prediction 218 grids (12-km horizontal resolution) from the 0000 UTC run of the North American Model. Lateral boundary conditions were specified at 3-h intervals and the simulation was run for 24 h. For brevity, only details from a portion of the 1-km domain are presented to compare with the King Air measurements and differential GPS isobaric height fields.

Figure 12 illustrates results from the WRF simulation at 2300 UTC, which corresponds to the time of the second King Air mapping mission (e.g., Fig. 11). This depiction covers roughly half the area of the inner domain, and focuses on the region where measurements from the King Air exist. Comparing Figs. 11 and 12 reveals that WRF is able to capture the essential features adjacent to Point Arguello.

The pattern of MBL height (Fig. 12a) to the north and west of Point Arguello is also similar to what previous King Air observations have indicated (e.g., Parish 2000). The height of the MBL decreases toward the continent and WRF simulations suggest MBL heights decrease from about 250 m on the western edge of the entire 1-km innermost domain (not shown in Fig. 12a) to less than 100 m just offshore in the relatively undisturbed MBL to the north of the Point Arguello headlands. As discussed by others (e.g., Zhang et al. 2011), simulated MBL heights are often shallower than observations suggest. This is also the case for 20 May 2012, even with the best boundary layer parameterization schemes.

MBL heights west of Point Arguello are between 150 and 200 m in WRF, but lidar observations indicated that the heights are closer to 300 m. WRF is not able to resolve the sharp temperature gradients at the MBL top that are readily detected in the King Air soundings such as those shown in Fig. 9. Even though there is a bias in height, the distribution of the MBL height from WRF is similar to the King Air observations. WRF simulations show the decrease of the MBL heights east of Point Arguello where MBL heights drop to under 75 m near Point Conception, similar to what was observed during the mapping mission.

WRF is also able to capture the prominent role of the Point Arguello headland in the MBL adjustment. The 995-hPa isobaric height field (Fig. 12b) reveals a confluence of contours at the Point Arguello headland. The locations of the strongest height gradients at 995 hPa in the 2300 UTC WRF output are similar to the differential GPS heights in Fig. 11, but the magnitudes of the gradients are slightly weaker than observed. Weaker height gradients in the simulation are consistent with the weaker simulated 995-hPa wind speeds (Fig. 12c). However, the wind directions and position of the wind maximum in the WRF output are similar to those observed.

Little evidence is found in the WRF simulation that suggests diffluence near the Point Arguello headland. This again implies that expansion fan dynamics may not be a dominant feature of the wind field. Potential temperatures at the 995-hPa level (Fig. 12d) display a pronounced increase east of Point Arguello of about 10 K over a horizontal distance of 10 km, matching the King Air observations. Interpretation of the large change in potential temperature is again that the 995-hPa surface passes through the temperature inversion at the top of the sloping MBL.

When compared with the King Air observations, the WRF simulation at a 1-km grid spacing reasonably

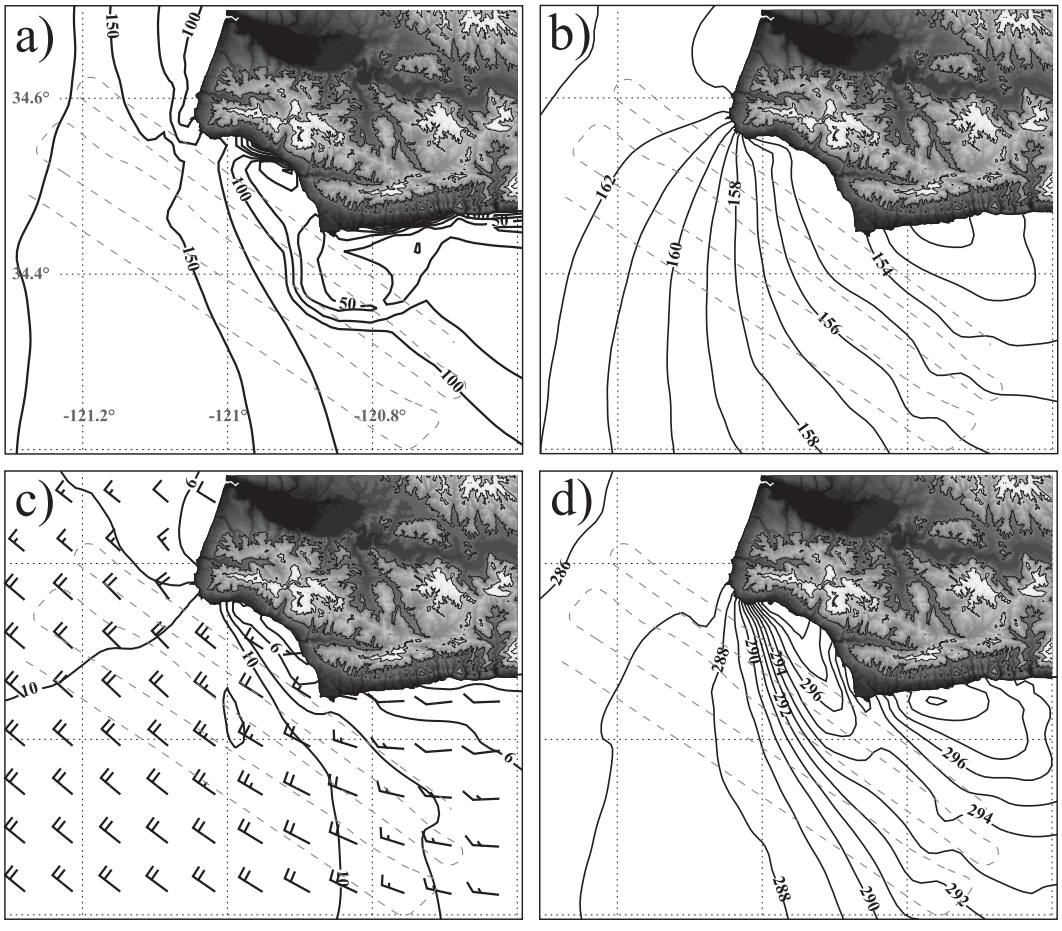

FIG. 12. As in Fig. 8, but from WRF simulation at 2300 UTC 20 May 2012 with dashed lines showing King Air flight track for second mapping.

captures the vertical structure of the wind and temperature and the collapse of the MBL to the east of Point Arguello. Figure 13 illustrates a cross section of the atmosphere at 2300 UTC, which is near the same time and along the same axis of the final leg of the second mapping mission and closest to the headlands. The isentropes (Fig. 13a) display a marked eastward descent with the strongest horizontal gradient near Point Arguello. This is in agreement with King Air observations such as those shown in Fig. 10d. The magnitude of the horizontal temperature change when passing across the MBL boundary is in general agreement with airborne observations, although the observed gradient is larger than that simulated by WRF. Measurements from the King Air suggest that the strongest change in potential temperatures, about 10 K, occurs over a horizontal distance about 5 km, whereas WRF simulates a more gradual change at the 995-hPa level that extends over half of the 20-km stretch between Point Arguello and Point Conception.

Spatial patterns of wind speed also match observations with the maximum speeds situated just east of Point Arguello, although simulated winds along the flight level of the King Air are approximately 3 m s^{-1} less than observed. WRF is able to correctly simulate the essence of the dynamics at work near Point Arguello. To show this, Fig. 13b depicts the isobaric perturbation heights that are computed by taking the difference between the actual isobaric height and the mean isobaric height at each level. The variation of these perturbation heights is a direct measure of the horizontal pressure gradient force like that illustrated in Fig. 10b. The magnitude of the isobaric height change as simulated by WRF at 995 hPa is about 12 m, which is only 3–4 m less than that observed by the King Air.

WRF captures the positioning of the strongest gradient just east of Point Arguello. Again, the simulation has issues with the intensity of the gradient, indicating a height decrease extending nearly to Point Conception. Observations of isobaric heights suggest that the gradient

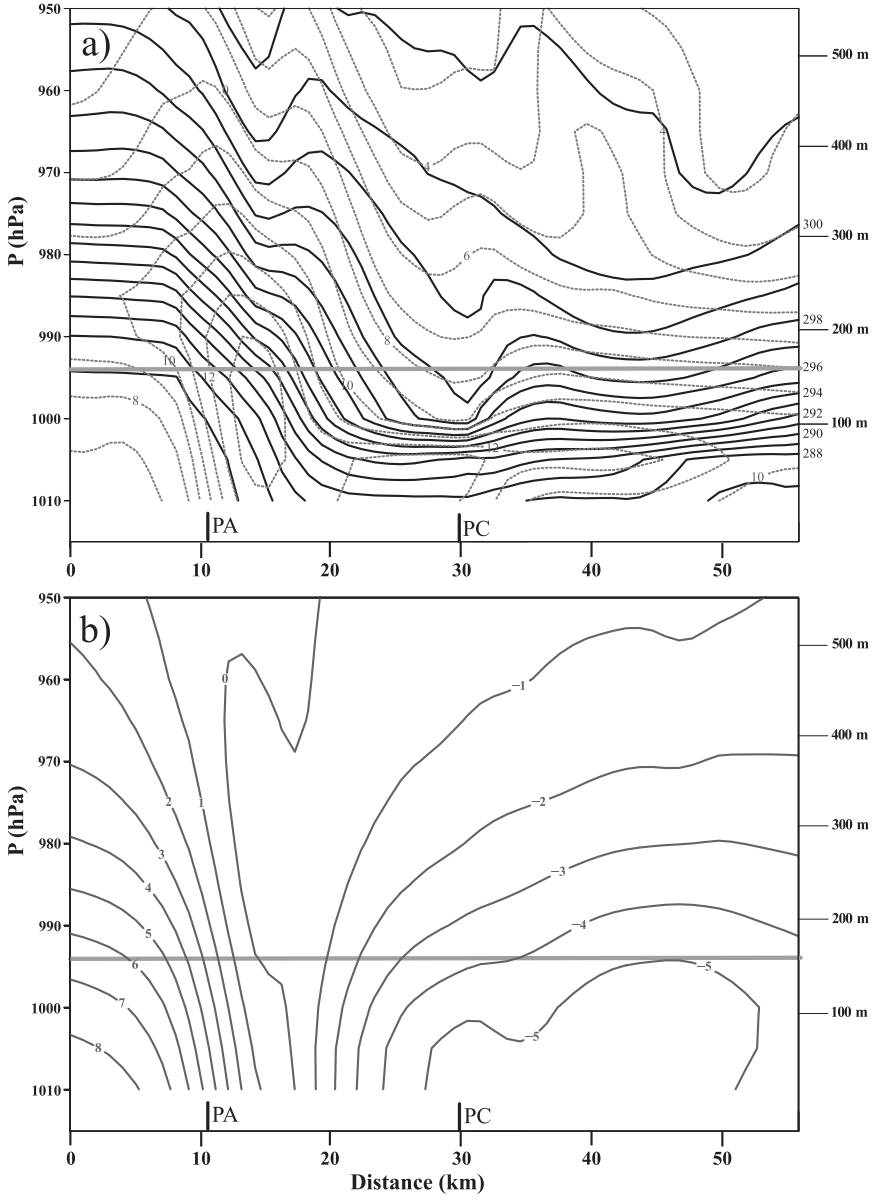

FIG. 13. Cross section from WRF simulation at 2300 UTC 20 May 2012 along King Air leg closest to Point Arguello–Point Conception headland in Fig. 1; (a) potential temperature (dark solid lines; K), wind speeds (light dashed lines; m s^{-1}) and (b) isobaric perturbation height field (m). Aircraft flight level is indicated by thick gray line; points closest to Point Arguello (PA) and Point Conception (PC) are indicated by solid tick marks on x axes.

begins to weaken about 5 km past Point Arguello. Although WRF simulations show MBL heights that are too low and cannot fully resolve the sharpest gradients in potential temperature and isobaric height, the pronounced atmospheric adjustment near Point Arguello is apparent.

5. Summary

Wind and temperature within the marine layer off the west coast of the United States have been the topic of extensive research during the past few decades. While significant progress has been made through modeling studies of the marine layer off the California coast, relatively few airborne measurements have been collected over the ocean near the Southern California coast close to Point Arguello. Observations from the King Air missions conducted during PreAMBLE provide some of the most detailed measurements of the adjustment of the marine layer to coastal topography. The 20 May 2012 case consists of moderate northerly wind in the MBL to the

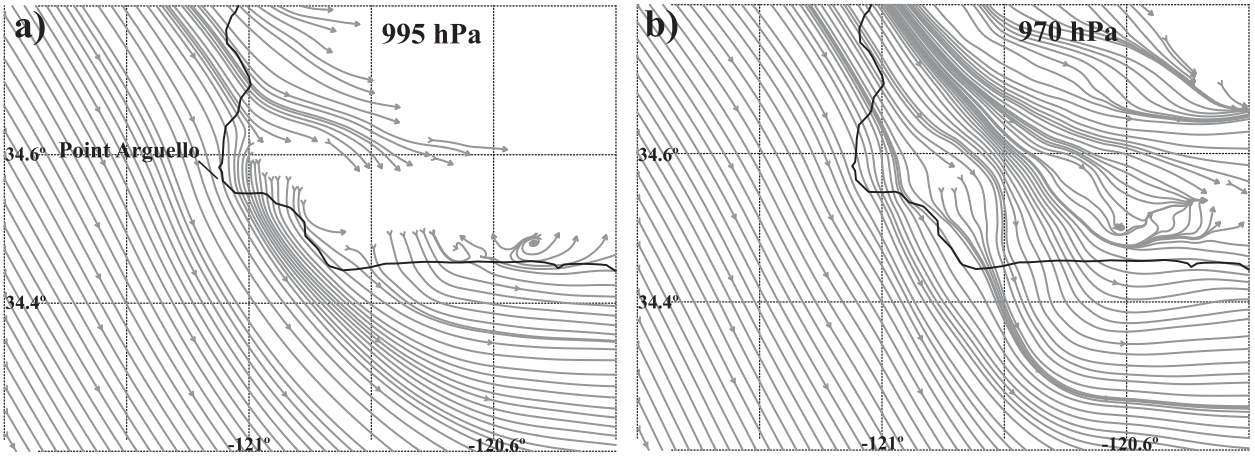

FIG. 14. Streamlines (solid gray lines) from WRF simulation at 2300 UTC 20 May 2012 at (a) 995 and (b) 970 hPa.

west of Point Arguello. Despite the cyclonic circulation evident in the morning, no easterly wind was observed in the Santa Barbara Channel at the time of the flight.

King Air observations at the 995-hPa level (corresponding to a height of about 150 m above the ocean) reveal an abrupt MBL transition near the Point Arguello headlands. Flow within the MBL prior to reaching Point Arguello is supercritical. As the low-level flow passes Point Arguello, MBL heights drop from over 300 m to less than 100 m over a horizontal distance of about 5 km. Large horizontal pressure gradients are associated with the sharp MBL transition and strongest 995-hPa winds are tied to the maximum height gradients.

The cause for the sudden MBL changes such as shown in Fig. 10 needs to be explained. Hydraulic theory has been used to describe a variety of MBL features. Dorman and Koračin (2008) have noted from their numerical studies that an expansion fan often forms near the Point Arguello–Point Conception headlands, resulting in an acceleration of the low-level flow that can extend over 100 km south.

For the 20 May 2012 case several factors argue against mechanical processes such as an expansion fan as the sole explanation of the MBL collapse. First, the 995-hPa wind fields from the King Air observations (Fig. 11c) and WRF output (Fig. 12c) show that no significant diffluence is present downwind of Point Arguello. Second, the lidar depolarization ratios provide information on the MBL structure and offer evidence of the nature and origin of air above the MBL.

Figure 10a provides compelling evidence that the air above the MBL contains large amounts of dry aerosol over a scale of about 20 km. PCASP total concentrations indicate a step change across the MBL frontal boundary in which aerosol concentrations change by a factor of 2–3 just east of Point Arguello. Such observations reflect aerosols having a continental origin. This region occurs above the MBL just after it collapses between Point Arguello and Point Conception. From Fig. 10, dry aerosol can be detected at levels in excess of 600 m east of Point Conception suggesting that the flow must be originating over the continent.

Results from WRF are consistent with this picture. Streamline analyses at the 995- and 970-hPa levels from the WRF simulation at 2300 UTC are shown in Fig. 14. The isentropic gradient from both King Air observations (Fig. 11d) and the WRF simulation (Fig. 12d) is the boundary between marine and continental air at 995 hPa (Fig. 14a). Flow is directed off the continent as depicted by the WRF results to the east of Point Arguello with streamlines parallel to the isentropes shown in Fig. 12d. Winds veer slightly with height such that the 970-hPa flow has a more pronounced northerly component, but the flow characteristics are consistent with continental aerosol as depicted in the lidar images and observed isobaric temperatures. Off-continent flow is present up to 900 hPa (not shown). The location of the MBL collapse is thus tied to off-continent transport of warm, dry air with lower momentum and a high concentration of aerosol.

A large isobaric height gradient occurs at the boundary between the cool marine layer and the warmer continental air. Hydrostatic considerations are sufficient to explain the isobaric height gradient. It is thus proposed that the horizontal pressure gradient force arises from the differing air masses.

The picture that emerges is that the MBL flow encounters a zone of enhanced low pressure resulting from the northerly offshore flow above the MBL east of Point Arguello that increases throughout the afternoon. Wind speeds increase where low pressure is encountered. From mass continuity arguments for open channel flow, the thickness of the MBL must decrease in response to the

acceleration. We propose that the pressure differential induces the pronounced change in the MBL height, similar to that of a spillway downstream from a weir where the elevation change forces dramatic flow characteristics. The fundamental cause for the MBL collapse on 20 May 2012 is therefore the acceleration induced by the horizontal pressure gradient that develops in response to the strong temperature contrast maintained by the differential temperature advection.

Acknowledgments. This research was supported in part by the National Science Foundation through Grant AGS-1034862. The authors thank pilots Ahmad Bandini and Brett Wadsworth and scientists Jeff French and Larry Oolman for help with the PreAMBLE field study and King Air measurements.

REFERENCES

Beardsley, R. C., C. E. Dorman, C. A. Friehe, L. K. Rosenfeld, and C. D. Winant, 1987: Local atmospheric forcing during the Coastal Ocean Dynamics Experiment: 1. A description of the marine boundary layer and atmospheric conditions over a northern California upwelling region. *J. Geophys. Res.,* **92,** 1467–1488, doi:10.1029/JC092iC02p01467.

Burk, S. D., and W. T. Thompson, 1996: The summertime low-level jet and marine boundary layer structure along the California coast. *Mon. Wea. Rev.,* **124,** 668–686, doi:10.1175/1520-0493(1996)124<0668:TSLLJA>2.0.CO;2.

——, T. Haack, and R. M. Samelson, 1999: Mesoscale simulation of supercritical, subcritical, and transcritical flow along coastal topography. *J. Atmos. Sci.,* **56,** 2780–2795, doi:10.1175/1520-0469(1999)056<2780:MSOSSA>2.0.CO;2.

Cai, Y., J. R. Snider, and P. Wechsler, 2013: Calibration of the passive cavity aerosol spectrometer probe for airborne determination of the size distribution. *Atmos. Meas. Tech. Discuss,* **6,** 4123–4152, doi:10.5194/amtd-6-4123-2013.

Dorman, C. E., 1985: Evidence of Kelvin waves in California's marine layer and related eddy generation. *Mon. Wea. Rev.,* **113,** 827–839, doi:10.1175/1520-0493(1985)113<0827:EOKWIC>2.0.CO;2.

——, and C. D. Winant, 2000: The marine layer in and around the Santa Barbara Channel. *Mon. Wea. Rev.,* **128,** 261–282, doi:10.1175/1520-0493(2000)128<0261:TSAVOT>2.0.CO;2.

——, and D. Koračin, 2008: Response of the summer marine layer flow to an extreme California coastal bend. *Mon. Wea. Rev.,* **136,** 2894–2922, doi:10.1175/2007MWR2336.1.

——, D. P. Rogers, W. Nuss, and W. T. Thompson, 1999: Adjustment of the summer marine boundary layer around Point Sur, California. *Mon. Wea. Rev.,* **127,** 2143–2159, doi:10.1175/1520-0493(1999)127<2143:AOTSMB>2.0.CO;2.

Edwards, K. A., A. M. Rogerson, C. D. Winant, and D. P. Rogers, 2001: Adjustment of the marine atmospheric boundary layer to a coastal cape. *J. Atmos. Sci.,* **58,** 1511–1528, doi:10.1175/1520-0469(2001)058<1511:AOTMAB>2.0.CO;2.

Haack, T., S. D. Burk, C. Dorman, and D. Rodgers, 2001: Supercritical flow interaction within the Cape Blanco–Cape Mendocino orographic complex. *Mon. Wea. Rev.,* **129,** 688–708, doi:10.1175/1520-0493(2001)129<0688:SFIWTC>2.0.CO;2.

Hsu, H.-M., L.-Y. Oey, W. Johnson, C. Dorman, and R. Hodur, 2007: Model wind over the central and southern California coastal ocean. *Mon. Wea. Rev.,* **135,** 1931–1944, doi:10.1175/MWR3389.1.

Koračin, D., and C. E. Dorman, 2001: Marine atmospheric boundary divergence and clouds along California in June 1996. *Mon. Wea. Rev.,* **129,** 2040–2056, doi:10.1175/1520-0493(2001)129<2040:MABLDA>2.0.CO;2.

——, ——, and E. P. Deaver, 2004: Coastal perturbations of marine-layer winds, wind stress, and wind stress curl along California and Baja California in June 1999. *J. Phys. Oceanogr.,* **34,** 1152–1172, doi:10.1175/1520-0485(2004)034<1152:CPOMWW>2.0.CO;2.

Lenschow, D. H., E. R. Miller, and R. B. Friesen, 1991: A three-aircraft comparison of two types of air motion measurement systems. *J. Atmos. Oceanic Technol.,* **8,** 41–50, doi:10.1175/1520-0426(1991)008<0041:ATAIOT>2.0.CO;2.

Parish, T. R., 2000: Forcing of the summertime low-level jet along the California coast. *J. Appl. Meteor.,* **39,** 2421–2433, doi:10.1175/1520-0450(2000)039<2421:FOTSLL>2.0.CO;2.

——, and D. Leon, 2013: Measurement of cloud perturbation pressures using an instrumented aircraft. *J. Atmos. Oceanic Technol.,* **30,** 215–229, doi:10.1175/JTECH-D-12-00011.1.

——, M. D. Burkhart, and A. R. Rodi, 2007: Determination of the horizontal pressure gradient force using global positioning system onboard an instrumented aircraft. *J. Atmos. Oceanic Technol.,* **24,** 521–528, doi:10.1175/JTECH1986.1.

——, D. A. Rahn, and D. Leon, 2013: Airborne observations of a Catalina eddy. *Mon. Wea. Rev.,* **141,** 3300–3313, doi:10.1175/MWR-D-13-00029.1.

Rahn, D. A., and T. R. Parish, 2007: Diagnosis of the forcing and structure of the coastal jet near Cape Mendocino using in situ observations and numerical simulations. *J. Appl. Meteor. Climatol,* **46,** 1455–1468, doi:10.1175/JAM2546.1.

——, and ——, 2008: A study of the forcing of the 22–25 June 2006 coastally trapped wind reversal based on numerical simulations and aircraft observations. *Mon. Wea. Rev.,* **136,** 4687–4708, doi:10.1175/2008MWR2361.1.

——, and ——, 2010: Cessation of the 22–25 June 2006 coastally trapped wind reversal. *J. Appl. Meteor. Climatol.,* **49,** 1412–1428, doi:10.1175/2010JAMC2242.1.

——, ——, and D. Leon, 2013: Airborne measurements of coastal jet transition around Point Conception, California. *Mon. Wea. Rev.,* **141,** 3827–3839, doi:10.1175/MWR-D-13-00030.1.

Rogers, D. P., and Coauthors, 1998: Highlights of Coastal Waves 1996. *Bull. Amer. Meteor. Soc.,* **79,** 1307–1326, doi:10.1175/1520-0477(1998)079<1307:HOCW>2.0.CO;2.

Saha, S., and Coauthors, 2010: The NCEP Climate Forecast System Reanalysis. *Bull. Amer. Meteor. Soc.,* **91,** 1015–1057, doi:10.1175/2010BAMS3001.1.

Samelson, R. M., 1992: Supercritical marine-layer flow along a smoothly varying coastline. *J. Atmos. Sci.,* **49,** 1571–1584, doi:10.1175/1520-0469(1992)049<1571:SMLFAA>2.0.CO;2.

——, and S. J. Lentz, 1994: The horizontal momentum balance in the marine atmospheric boundary layer during CODE-2. *J. Atmos. Sci.,* **51,** 3745–3757, doi:10.1175/1520-0469(1994)051<3745:THMBIT>2.0.CO;2.

Skamarock, W. C., and Coauthors, 2008: A description of the Advanced Research WRF version 3. NCAR Tech. Note NCAR/TN-475+STR, 113 pp. [Available online at http://www.mmm.ucar.edu/wrf/users/docs/arw_v3_bw.pdf.]

Skyllingstad, E. D., P. Barbour, and C. E. Dorman, 2001: The dynamics of northwest summer winds over the Santa Barbara Channel. *Mon. Wea. Rev.,* **129,** 1042–1061, doi:10.1175/1520-0493(2001)129<1042:TDONSW>2.0.CO;2.

Wang, Z., P. Wechsler, W. Kuestner, J. French, A. R. Rodi, B. Glover, M. Burkhart, and D. Lukens, 2009: Wyoming Cloud Lidar: Instrument description and applications. *Opt. Express,* **17,** 13 576–13 587, doi:10.1364/OE.17.013576.

——, J. French, G. Vali, and P. Wechsler, 2012: Single aircraft integration of remote sensing and in situ sampling for the study of cloud microphysics and dynamics. *Bull. Amer. Meteor. Soc.,* **93,** 653–668, doi:10.1175/BAMS-D-11-00044.1.

Winant, C. D., C. E. Dorman, C. A. Friehe, and R. C. Beardsley, 1988: The marine boundary layer off northern California: An example of supercritical channel flow. *J. Atmos. Sci.,* **45,** 3588–3605, doi:10.1175/1520-0469(1988)045<3588:TMLONC>2.0.CO;2.

Zemba, J., and C. A. Friehe, 1987: The marine boundary layer jet in the Coastal Ocean Dynamics Experiment. *J. Geophys. Res.,* **92,** 1489–1496, doi:10.1029/JC092iC02p01489.

Zhang, C., Y. Wang, and K. Hamilton, 2011: Improved representation of boundary layer clouds over the southeast Pacific in ARW-WRF using a modified Tiedtke cumulus parameterization scheme. *Mon. Wea. Rev.,* **139,** 3489–3512, doi:10.1175/MWR-D-10-05091.1.